Title	Facile synthesis of monodispersed silver nanoparticles on graphene oxide sheets with enhanced antibacterial activity(main article)
Author(s)	Liu, Lei; Liu, Jincheng; Wang, Yinjie; Yan, Xiaoli; Sun, Darren Delai
Citation	Liu, L., Liu, J., Wang, Y., Yan, X. & Sun, D. D. (2011). Facile synthesis of monodispersed silver nanoparticles on graphene oxide sheets with enhanced antibacterial activity. New Journal of Chemistry, 35(7), 1418-1423.
Date	2011
URL	http://hdl.handle.net/10220/7473
Rights	© 2011 The Royal Society of Chemistry and the Centre National de la Recherche Scientifique. This is the author created version of a work that has been peer reviewed and accepted for publication by New Journal of Chemistry, The Royal Society of Chemistry and the Centre National de la Recherche Scientifique. It incorporates referee's comments but changes resulting from the publishing process, such as copyediting, structural formatting, may not be reflected in this document. The published version is available at: [DOI: http://dx.doi.org/10.1039/C1NJ20076C]

NJC

Dynamic Article Links ►

Cite this: DOI: 10.1039/c0xx00000x

www.rsc.org/xxxxxx

ARTICLE TYPE

Facile Synthesis of Monodispersed Silver Nanoparticles on Graphene Oxide Sheets with Enhanced Antibacterial Activity

Lei Liu,[a] Jincheng Liu,*[a] Yinjie Wang,[a] Xiaoli Yan,[a] and Darren Delai Sun*[a]

Received (in XXX, XXX) Xth XXXXXXXXX 20XX, Accepted Xth XXXXXXXXX 20XX

DOI: 10.1039/b000000x

Table of contents entry

Highly monodispersed Ag nanoparticles have been successfully anchored on the graphene oxide sheets by a facile two-phase synthesis.

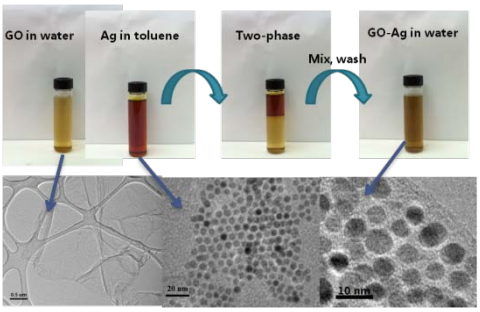

Graphene oxide-Ag nanoparticle (GO-Ag) composites were synthesized through a facile two-phase (toluene-water) process. Transmission Electron Microscope and X-ray diffraction analysis revealed that the Ag nanoparticles anchored on GO sheets were spherical in shape and highly monodispersed with uniform size of 6 nm. The antibacterial activity of GO-Ag composites was investigated against gram-negative bacteria *Escherichia coli* (*E.coli*) and showed a remarkably enhanced antibacterial activity compared with the original Ag nanoparticles, suggesting that the as-prepared nanocomposites may be used as effective antibacterial materials

Introduction

Silver (Ag) nanoparticles are known to exhibit the highest bactericidal activity and biocompatibility amongst all the antibacterial nanomaterials.[1-3] It has been reported that Ag nanoparticles and hybrid Ag nanocomposites are shown to be effective biocides against numerous kinds of bacteria, fungi and virus.[2] Due to their promising antibacterial capability, Ag nanoparticles have attracted numerous studies on its application as an antiseptic, disinfectant and pharmaceutical agent.[4-6] Studies have shown that the toxicity of Ag nanoparticles is size dependent and the smaller sized exhibit higher antibacterial activity (< 10 nm), due to the high specific surface area and easy cell penetration.[2, 3] Therefore, monodispersed Ag nanoparticles with small size are desirable for the antibacterial control system. Nevertheless, the particle aggregation problem and nanomaterial recovery are two big challenges of using Ag nanoparticles in applications.

Graphene has been the major focus of recent research to exploit a sp^2-hybrid carbon network.[7] In particular, graphene is considered as an ideal two-dimensional reinforcing component for composite materials possessing superior carrier transport, high mechanical stiffness, extremely large surface area and fine thermal/chemical stability.[7-9] Graphene oxide (GO) is a chemically modified graphene with hydroxyl and carboxyl groups, which has high water solubility.[9] The new graphene-based hybrids with metal nanoparticles such as Pt, Au and Ag have shown potential applications in the area of optics, electronics, catalysis and sensors.[10-13] However, information of biological studies on graphene-based composites is still insufficient. Recent research reported that GO is a relative biocompatible material.[14] Shen et al. (2010) illustrated that Ag nanoparticles retain good antibacterial activity on GO sheet.[15] Very recently, Das et al. (2011) reported that the antibacterial activity of Ag nanoparticles on GO is size and shape dependent, and Ma et al. (2011) reported a synergistic effect of GO and Ag nanoparticles.[16, 17] Thus, GO-Ag composites are supposed to be effective antibacterial materials, which possess the specific properties of both GO and

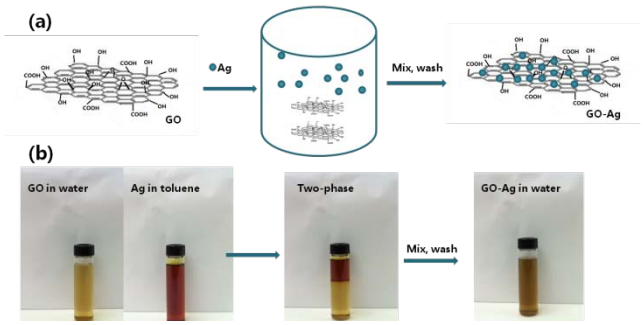

Scheme 1 Steps for the synthesis of the GO-Ag composites: (a) Schematic presentation of the two-phase synthesis of GO-Ag composites; (b) Photographs of the two-phase synthesis of GO-Ag composites.

Ag nanoparticles. The synthesis of GO-Ag composites has been reported by several researchers, mostly using a solution-based single-step method to reduce Ag^+ ions on GO sheets.[15-21] However, this single-step approach has difficulty in controlling the morphology and size of Ag nanoparticles on GO sheets, because Ag nanoparticles are formed onto GO sheets directly during Ag^+ ion reduction. Since the antibacterial activity of Ag nanoparticles relies heavily on its size, precise size control of the Ag nanoparticles anchored on GO sheets is essential. One recent work reported a dry decoration of GO with Ag nanocrystals from an arc plasma source using electrostatic force.[22] However, the use of extra electric field limits its broad application in reality. Our previous work has successfully synthesized GO-TiO_2 composites by a facile two-phase self-assembling approach,[23] and it is proved that this method is suitable for the assembling of high-quality organically soluble nanocrystals on the GO sheets.

In this work, a facile two-phase method that embeds Ag nanoparticles onto GO sheets is reported. It is worth to be highlighted that this method can successfully anchor highly monodispersed Ag nanoparticles on GO sheets at the water/toluene interface. It is a remarkable advancement for the existing methods of synthesis of GO-Ag composites, and can provide a universal approach for the synthesis of high quality GO-metal composites. Moreover, assembling the Ag nanoparticles on large GO sheets can remarkably enhance the antibacterial activity and facilitate the recovery by simple filtration, which is beneficial for the applications in environmental engineering and other fields.

Experimental

Preparation and Characterization of GO-Ag Composites

Natural graphite (SP1) was purchased from Bay Carbon Company (USA). Soudium nitrate ($NaNO_3$, 99%), potassium permanganate ($KMnO_4$, 99%), hydrogen peroxide (H_2O_2, 35%), concentrated sulfuric acid (36.5%), oleic acid (OLA, 99%), and silver nitrate ($AgNO_3$, 99%) were purchased from Sigma-Aldrich.

Toluene, acetone, ethanol (absolute), and tetrahydrofuran (THF) were purchased from Merk Ltd (Singapore). All reagents were used without further purification.

GO was synthesized according to the modification of Hummers' method from natural graphite, and the process was described earlier.[24, 25] Oleylamine-capped Ag nanoparticles were synthesized by reducing $AgNO_3$ in toluene, which was described previously.[26] GO (15 mg) and DI water (100 ml) were added into a bottle (250 mL) and sonicated for 1 h before use. Ag nanoparticles (45 mg) dispersed in toluene (50 mL) were added into the GO water solution. The mixture was kept stirring for 12 h at room temperature to ensure Ag nanoparticles coordinated with GO sheets at the water/toluene interface. The GO-Ag composites were purified with acetone and centrifuged at 10 000rpm for 10 min. The obtained GO-Ag composites were then washed by THF to get rid of residual oleylamine on the Ag nanoparticles. The total process can be illustrated as Scheme 1a. The final GO-Ag composites were freeze dried at -50°C for 24 h.

Atomic force microscopy (AFM) was carried out using a non-contact mode on a PSIA XE-150 scanning probe microscope. The AFM sample was prepared by spin coating the dispersion water solution of GO onto Si substrate covered with 300 nm thick SiO_2. Transmission electron microscopy (TEM) and high-resolution TEM (HRTEM) images were obtained using a JEOL 2010-H microscope operating at 200 kV. The samples for the analysis were prepared by dropping dilute toluene solution of oleylamine-capped Ag nanoparticles, GO water solution and GO-Ag water solution. X-ray powder diffraction (XRD) patterns were taken on a D8-Advance Bruker-AXS diffractometer using Cu Kα irradiation. X-ray photoelectron spectroscopy (XPS) measurements were carried out by using a Kratos Axis Ultra Spectrometer with a monochromic Al Ka source at 1486.7 eV, with a voltage of 15 kV and an emission current of 10 mA.

Bacterial Culture

Escherichia coli (E.coli) K12 ER2925 (New England Biolab) was chosen as the model pathogen for antibacterial activity experiments. *E.coli* was cultivated in Luria-Bertani nutrient solution at 37°C for 18h to get the exponential growth phase. The cells were harvested by centrifugation and washed with saline solution (0.9% NaCl) to remove residual macromolecules. The cells were re-suspended in a saline solution to maintain the concentration of 10^7-10^8 colony forming units (cfu/mL). All glass apparatuses and solutions used in the experiments were autoclaved at 121°C for 20min to ensure sterility.

Antibacterial Activity Test

E.coli cells were inoculated in saline solution containing 0, 20, 50, 80, 100 μg/mL of GO, Ag nanoparticles and GO-Ag composites, respectively, with a final cell concentration around 10^7 cfu/mL. The mixture was incubated with gentle shaking for 2 h at 37°C. The mixture was diluted with a gradient method and then applied uniformly on three LB culture medium plates per gradient solution. These plates were incubated at 37°C for 24 h. The colony forming units were counted and compared with control plates to calculate percentage of cell viability (C/C_0). Meanwhile, at the concentration of 100 μg/mL of GO, Ag nanoparticles and GO-Ag composites, the mixture was taken out at reaction time 0, 30, 60, 90 and 120 min to measure the time course of the antibacterial activity of samples.

The antibacterial activity of GO-Ag composites was further verified by LIVE/DEAD BacLight bacterial viability assay (Invitrogen, USA). SYTO 9 and propidium iodide (PI) stock solutions from the assay kit were combined with an equal volume

to add to the *E.coli* solution after 2 h incubation with 100 μg/mL of GO, Ag nanoparticles and GO-Ag composites, respectively. The mixtures were incubated at room temperature in the dark for 15 min and then observed by Leica TCS SP5 laser scanning confocal microscope (Leica Microsystems, Germany).

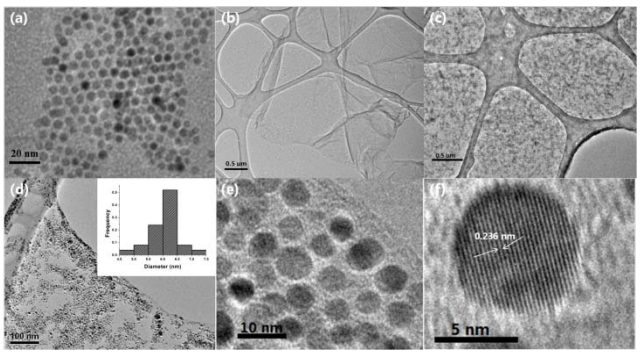

Fig.1 TEM images of Ag nanoparticles (a), GO sheets (b), GO-Ag composites ((c), (d), (e) and (f)). Inset of (d) is the size distribution of Ag nanoparticles on GO sheets.

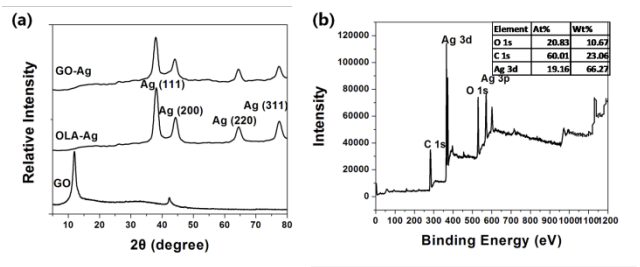

Fig. 2 (a) XRD patterns of GO sheets, oleylamine-capped Ag nanoparticles and GO-Ag composites. (b) XPS spectra of GO-Ag composites (Inset table is the element weight percentage).

The morphological changes of *E.coli* were investigated by scanning electron microscopy (SEM, JEOL, 6340). After filtering the *E.coli* mixture with glass filter, the cells on the filter were quickly fixed with 2% glutaraldehyde and 1% osmium tetroxide. Then the cells on the filter were dehydrated with sequential treatment with 50, 70, 85, 90 and 100% ethanol for 10 min. The filter was freeze dried at -50°C before test.

Results and Discussion

Preparation and Characterization of GO-Ag Composites

The morphology and size of the oleylamine-capped Ag nanoparticles could be well-controlled via the organic phase synthesis.[26, 27] Oleylamine-capped Ag nanoparticles were well dispersed in toluene, while hydrophilic GO sheets were well dispersed in deionized (DI) water, as shown in photographs of Scheme 1b. The aqueous solution of GO and the toluene solution of Ag nanoparticles were mixed and stirred for 12 h to ensure the self-assembly of Ag nanoparticles onto the GO sheets in the water/toluene interface. It has been reported that metal nanoparticles can interact with the GO sheets through electrostatic binding, physisorption and charge-transfer interactions.[13] Meanwhile, the large GO sheets act as excellent support and stabilizer for the Ag nanoparticles, avoiding nanoparticle aggregation. After centrifugation of the mixture and washing off extra oleylamine, the pure GO-Ag composites can be formed and well dispersed in water as shown in Scheme 1b. The hydrophilic property to the GO-Ag composites is ascribed to the carboxyl and hydroxyl groups of the GO sheets. This two-phase method is facile and reproducible to be widely used for the synthesis of other GO-metal composites.

AFM was used to verify the numbers of GO layer synthesized. An AFM image of GO sheets is shown in Figure S1. From the two line scans, the thickness of GO sheets is measured around 1.2 nm, which is slightly larger due to the oxygen groups than reported apparent thickness of single-sheet graphene.[28] The measured thickness of GO assures that the GO is exfoliated into single sheets in water. The TEM was used to analyze the morphology of GO-Ag composites. Figure 1a shows that oleylamine-capped Ag nanoparticles synthesized in toluene are highly monodispersed with a uniform size of 6 nm, which are able to provide super antibacterial capability. Figure 1b illustrates that the size of the GO sheets synthesized is larger than 2 μm. Since the potential cytotoxicity of engineered nanomaterials is of significant consideration when they are exposed to the environment,[29, 30] the GO sheets with a large size may benefit the recovery of GO-Ag composite materials after disinfection by simple filtration. The GO sheets are uniformly covered by Ag nanoparticles as is shown in Figures 1c and 1d. The image in Figure 1d reveals a single GO-Ag composite sheet. It can be observed clearly that Ag nanoparticles are well monodispersed on GO sheet without any aggregation. Both the edge of GO sheet and the nanostructure of the Ag nanoparticles are clearly observable in the higher magnification of Figure 1e, while there are no Ag nanoparticles outside the GO sheets. Figure 1f gives the high-resolution TEM images of GO-Ag composites from Figure 1e. The measured lattice-fringe spacing of the nanoparticles is 0.236 nm, which is corresponding to the (111) crystal plane of Ag nanoparticles. These images of TEM confirm that the highly monodispersed Ag nanoparticles with uniform size around 6 nm are successfully synthesized and well located on GO sheets by the two-phase approach. Compared with the reported works, our Ag nanoparticles on GO sheets seem to be highly monodispersed with smaller uniform size.[15-17]

To further validate the Ag nanoparticles anchored onto the GO sheets and to value the mass ratio of Ag/GO, XRD and XPS were applied to measurements. Figure 2a shows the XRD patterns of GO sheets, oleylamine-capped Ag nanoparticles and GO-Ag composites. The curve of GO sheets shows a diffraction peak at 2θ value around 11.9°, which may be due to interlamellar water trapped between hydrophilic graphene oxide sheets.[31] In the curve of oleylamine-capped Ag nanoparticles, the clear peaks at 2θ values of about 38.1°, 44.3°, 64.5° and 77.5° are assigned to the (111), (200), (220), and (311) crystallographic planes of face-centered cubic (fcc) Ag nanoparticles, respectively (JCPDS No. 07-0783). The average size of the Ag nanoparticles was calculated to be 6.6 nm from Ag (111) peak based on Scherrer's equation. The curve of GO-Ag composites is without changes in comparison with Ag nanoparticles. No obvious diffraction peaks of GO were observed in the GO-Ag composites, because the regular stack of GO was destroyed by the intercalation of Ag nanoparticles, which is consistent with other reported works about GO-metal composites.[15, 16, 32] The crystallite size of Ag

nanoparticles on GO sheets was calculated to be 7.2 nm, which is in good agreement with the result of TEM. The XRD results confirm the Ag nanoparticles have successfully located onto the GO sheets. The XPS spectrum of GO-Ag composites in Figure 2b shows the major element peaks belong to C 1s, O 1s and Ag 3d, respectively. The weight percentage of each element was

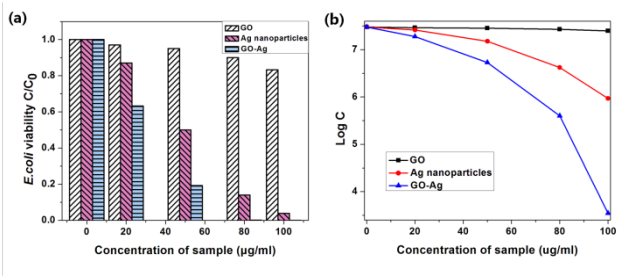

Fig.3 Antibacterial activity of GO sheets, Ag nanoparticles and GO-Ag composites at different concentration with the initial *E.coli* concentration of $3*10^7$ cfu/mL: (a) *E.coli* viability percentage; (b) Log *E.coli* viability.

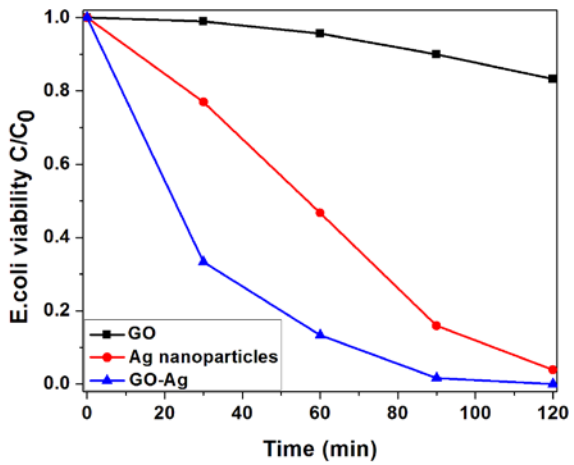

Fig.4 Time course for antibacterial activity of 100 μg/mL of GO sheets, Ag nanoparticles and GO-Ag composites, with an initial *E.coli* concentration of $3*10^7$ cfu/mL

analyzed by CasaXPS software according to the peaks, as shown in the inset of Figure 2b. The weight percentage of Ag nanoparticles in GO-Ag composites is 66.27%, illustrating the mass ratio of Ag/GO is about 2/1.

Antibacterial Activity of GO-Ag Composites

The antibacterial activity of GO-Ag composites was evaluated by a colony forming count method. *E.coli* was chosen as the model waterborne pathogen in this experiment. Figure 3a shows that with the increase of the concentration of GO-Ag composites, the number of bacteria decreases dramatically; 99% of *E.coli* cells have been killed at the concentration of 80 μg/mL. The results demonstrate that the GO-Ag composites have high-performance antibacterial capability at relatively low concentration. In control experiments, the antibacterial activity of pure GO sheets and pure Ag nanoparticles were also tested. The pure GO sheets show low antibacterial activity to *E.coli* cells; 10% of *E.coli* cells have been inactivated at the concentration of 80 μg/mL, and 17% at the concentration of 100 μg/mL(Figure 3a). This result differs from the recent published report which concludes that GO has high antibacterial activity for *E.coli*.[14] Possible reason for this phenomenon is that GO sheets used in this study have different oxygen-containing group content compared with those they used, which may affect the interaction between GO and bacteria cells. Figure 3a shows that pure Ag nanoparticles have good antibacterial activity; 86% of *E.coli* cells have been killed at the

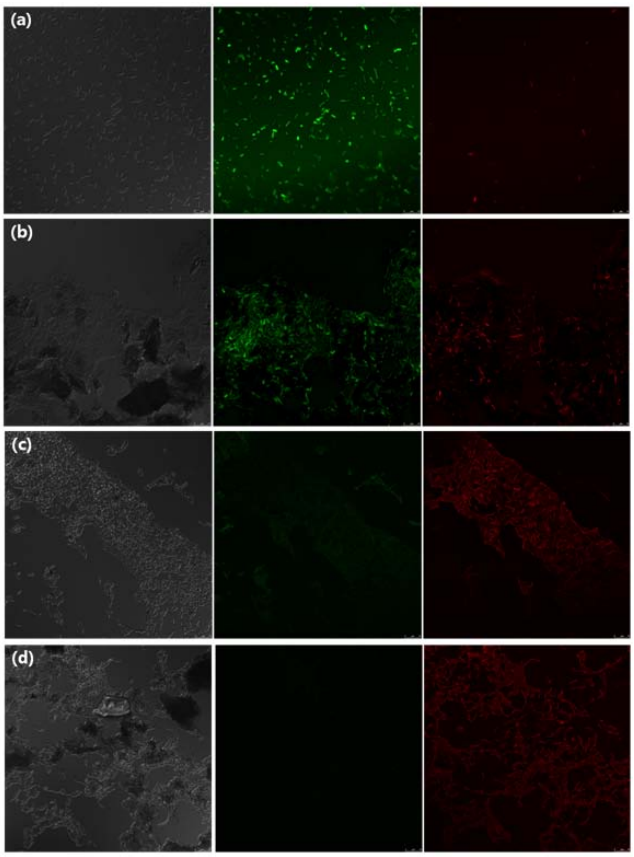

Fig. 5 Real microscopic images and fluorescence microscopic images of bacteria after incubation with different samples in saline solution for 2 h: (a) *E.coli* without samples; (b) *E.coli* with 100 μg/mL of GO sheets; (c) *E.coli* with 100 μg/mL of Ag nanoparticles; (d) *E.coli* with 100 μg/mL of GO-Ag composites.

concentration of 80 μg/mL, and 96% at the concentration of 100 μg/mL. This result reveals that the pure Ag nanoparticles synthesized here have effective antibacterial activity, and they contribute the major part to the antibacterial capability of GO-Ag composites. To clearly find out the difference of antibacterial efficiency between the pure Ag nanoparticles and GO-Ag composites, the real number of *E.coli* (initial concentration of $3*10^7$ cfu/mL) to be inactivated is counted according to the concentration of samples, as is shown in Figure 3b. GO sheets itself shows nearly no log decrease of *E.coli* cells at the concentration of 100 μg/mL, and Ag nanoparticles shows 1.5 log decrease of *E.coli* cells at the same concentration. However, GO-Ag composites show 4 log decrease of *E.coli* cells at the concentration of 100 μg/mL. The results clearly illustrate that at the same concentration, pure GO sheets shows little antibacterial activity, while GO-Ag composites have much higher antibacterial activity than pure Ag nanoparticles. Considering that the real percentage of Ag nanoparticles of GO-Ag composites is about

66%, which means that 100 μg/mL of GO-Ag composites equal to 66 μg/mL of Ag nanoparticles, we can conclude that GO-Ag composites display remarkable enhanced antibacterial activity compared to pure Ag nanoparticles.

The time course for the *E.coli* inactivation was investigated to find out the disinfection rate of GO-Ag composites. It can be seen in Figure 4 that at the same concentration, GO-Ag composites illustrate the highest disinfection rate compared to pure GO and

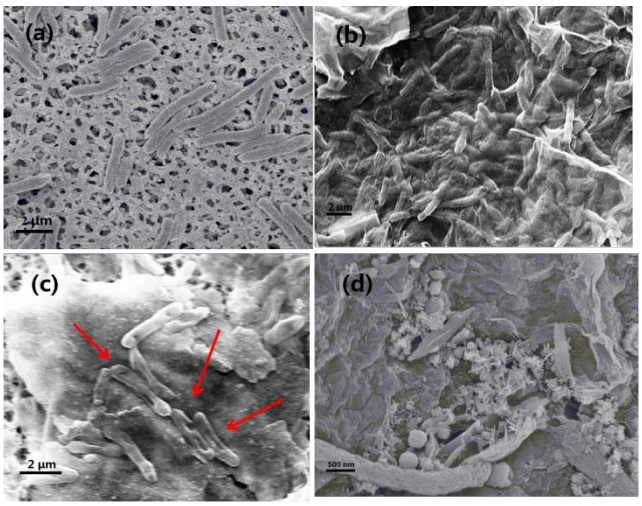

Fig.6 SEM images of *E.coli* after membrane filtration with different concentration of GO-Ag composites: (a) 0 μg/mL, (b) 20 μg/mL, (c) 50 μg/mL, (d) 100 μg/mL.

pure Ag nanoparticles. This result agrees with the results obtained above to further confirm that GO-Ag composites have enhanced antibacterial activity compared to pure GO and pure Ag nanoparticles.

To verify the reliability of the colony forming count method in this particular study, we further examined the antibacterial activity of GO-Ag composites by a LIVE/DEAD BacLight bacterial viability kit. With an appropriate mixture of the SYTO 9 and propidium iodide (PI), bacteria with intact cell membranes stain fluorescent green, whereas bacteria with damaged membranes stain fluorescent red. The real images of bacteria can be recorded as well by the microscope at the same time. Figure 5a shows that *E.coli* in control experiment dispersed well in saline solution, and most of the *E.coli* survived with green color. After incubation with GO, *E.coli* cells have aggregated together on the GO sheets as shown in real image of Figure 5b. However, most of the *E.coli* cells were still alive to exhibit green color, which confirms that GO sheets have low toxicity to *E.coli*. Figure 5c provides the images of *E.coli* in the presence of 100 μg/mL Ag nanoparticles, showing that most of the *E.coli* cells were dead with red color. Figure 5d shows that nearly all the *E.coli* cells were inactivated to exhibit red color at the concentration of 100 μg/mL GO-Ag composites. The fluorescence-based assay is in good agreement with the results obtained by the colony forming count method. Therefore, we can conclude that GO itself has lower antibacterial activity, and pure Ag nanoparticles have higher antibacterial activity towards *E.coli* at the size of 6 nm. The GO sheets and Ag nanoparticles show synergetic effect on antibacterial activity when they combine into GO-Ag composites.

Recovery of the nanomaterials is essential to avoid nano-toxicity to the ecosystem. The glass filter with pore size of 0.45 μm was applied here for membrane filtration after disinfection. The scanning electron microscopy (SEM) was used to investigate the morphology of *E.coli* cells after disinfection and membrane filtration process. Without GO-Ag composites, *E.coli* cells remained in good state as shown in Figure 6a. However, with the increasing dosage of GO-Ag composites, the damage of the *E.coli* cells increased, which are illustrated from Figures 6b to 6d. Figure 6b reveals that GO sheets could obviously adsorb *E.coli* cells together. In the presence of 20 μg/mL GO-Ag composites, most of the *E.coli* cells gathered on the GO sheets remained to be in good state. In the presence of 50 μg/mL of GO-Ag composite, the image of the *E.coli* cells on the GO-Ag composites reveals that the cell walls of the bacteria have been damaged significantly, as shown in Figure 6c. At the concentration of 100 μg/mL GO-Ag composites, most of the bacteria in solution were destroyed into pieces as shown in Figure 6d. The SEM results imply the possible mechanism of antibacterial activity of GO-Ag composites: Firstly, the water soluble GO sheets adsorb and gather the bacteria onto the surface, which may enhance the interaction between bacteria and Ag nanoparticles on GO sheets. Some research has reported that GO sheets show high non-specific binding capability to microbes.[33] Secondly, Ag nanoparticles damage the bacterial cell wall when contact with the bacteria. Eventually the bacteria can be destroyed into pieces. Obviously, Ag nanoparticles play the key role in the antibacterial process. However, pure Ag nanoparticles show much lower antibacterial activity than GO-Ag composites. It may be due to the aggregation of pure Ag nanoparticles during antibacterial process, leading to the reduction of active specific surface area of Ag nanoparticles. Moreover, pure Ag nanoparticles modified with surfactant may prevent silver ion releasing, and then prevent adhesion of Ag nanoparticles to the bacterial cell surface.[2] On the contrary, GO sheets play a positive role in the adhesion of bacterial to the surface of the GO-Ag composites, which could remarkably increase the interaction between the Ag nanoparticles and the bacterial surface. Since the GO-Ag composites show effective antibacterial activity to the bacteria, it can also be applied as the anti-biofouling agents, as the formation of biofilm is one of the major problems in membrane filtration process in water treatment industry.[34] Meanwhile, the images of SEM reveal that GO-Ag composites can be easily recovered from treated water by filtration without leaving disinfection material pollutant behind.

Conclusions

In summary, monodispersed Ag nanoparticles were anchored successfully on large GO sheets by a facile two-phase assembling method. The GO-Ag composites show remarkably enhanced antibacterial activity towards *E.coli* compared to the original Ag nanoparticles. The high-performance disinfection property of GO-Ag composites may be due to the adsorption of the bacteria by GO sheets through non-specific binding. The GO sheets can effectively stabilize Ag nanoparticles to prevent their aggregation. The recovery of GO-Ag composites can be implemented by a simple filtration process due to the large GO sheets. Given the superior antibacterial activity of GO-Ag

composites and the fact that GO-Ag composites can be easily recovered, we expect this new composite could offer promising opportunities in the applications of the environment engineering and other fields.

Acknowledgements

Authors would like to acknowledge the Clean Energy Research Programme under National Research Foundation of Singapore and the Singapore Environment & Water Industry (EWI) Development Council for their research grant (Grant No. NRF2007EWT-CERP01-0420 and MEWR 651/06/166) support for this work.

Notes and references

[a] *School of Civil and Environmental Engineering, Nanyang Technological University, Block N1, Nanyang Avenue, Singapore 639798*
Corresponding Email: JCLIU@ntu.edu.sg; DDSUN@ntu.edu.sg
† Electronic Supplementary Information (ESI) available: Additional figure, AFM of GO sheets. See DOI: 10.1039/b000000x/

1. M. L. W. Knetsch and L. H. Koole, *Polymers*, 2011, **3**, 340.
2. C. Marambio-Jones and E. M. V. Hoek, *J. Nanopart. Res.*, 2010, **12**, 1531.
3. J. R. Morones, J. L. Elechiguerra, A. Camacho, K. Holt, J. B. Kouri, J. T. Ramirez and M. J. Yacaman, *Nanotechnology*, 2005, **16**, 2346.
4. A. Kumar, P. K. Vemula, P. M. Ajayan and G. John, *Nat. Mater.*, 2008, **7**, 236.
5. V. A. Oyanedel-Craver and J. A. Smith, *Environ. Sci. Technol.*, 2008, **42**, 927.
6. S. Pal, E. J. Yoon, Y. K. Tak, E. C. Choi and J. M. Song, *J. Am. Chem. Soc.*, 2009, **131**, 16147.
7. A. K. Geim, *Science*, 2009, **324**, 1530.
8. C. Lee, X. D. Wei, J. W. Kysar and J. Hone, *Science*, 2008, **321**, 385.
9. D. A. Dikin, S. Stankovich, E. J. Zimney, R. D. Piner, G. H. B. Dommett, G. Evmenenko, S. T. Nguyen and R. S. Ruoff, *Nature*, 2007, **448**, 457.
10. Y. G. Zhou, J. J. Chen, F. B. Wang, Z. H. Sheng and X. H. Xia, *Chem. Commun.*, 2010, **46**, 5951.
11. R. Pasricha, S. Gupta and A. K. Srivastava, *Small*, 2009, **5**, 2253.
12. I. V. Lightcap, T. H. Kosel and P. V. Kamat, *Nano Lett.*, 2010, **10**, 577.
13. R. Muszynski, B. Seger and P. V. Kamat, *J. Phys. Chem. C*, 2008, **112**, 5263.
14. W. B. Hu, C. Peng, W. J. Luo, M. Lv, X. M. Li, D. Li, Q. Huang and C. H. Fan, *ACS Nano*, 2010, **4**, 4317.
15. J. F. Shen, M. Shi, N. Li, B. Yan, H. W. Ma, Y. Z. Hu and M. X. Ye, *Nano Res.*, 2010, **3**, 339.
16. M. R. Das, R. K. Sarma, R. Saikia, V. S. Kale, M. V. Shelke and P. Sengupta, *Colloids and Surfaces B: Biointerfaces*, 2011, **83**, 16.
17. J. Ma, J. Zhang, Z. Xiong, Y. Yong and X. S. Zhao, *J. Mater. Chem.*, 2011, **21**, 3350-3352.
18. H. W. Tien, Y. L. Huang, S. Y. Yang, J. Y. Wang and C. C. M. Ma, *Carbon*, 2011, **49**, 1550.
19. Z. Tang, S. Shen, J. Zhuang and X. Wang, *Angewandte Chemie - International Edition*, 2010, **49**, 4603.
20. X. Z. Zhou, X. Huang, X. Y. Qi, S. X. Wu, C. Xue, F. Y. C. Boey, Q. Y. Yan, P. Chen and H. Zhang, *J. Phys. Chem. C*, 2009, **113**, 10842.
21. C. Xu and X. Wang, *Small*, 2009, **5**, 2212.
22. G. H. Lu, S. Mao, S. Park, R. S. Ruoff and J. H. Chen, *Nano Res.*, 2009, **2**, 192.
23 J. Liu, H. Bai, Y. Wang, Z. Liu, X. Zhang and D. D. Sun, *Adv. Funct. Mater.* 2010, **20**, 4175.
24. J. Liu, H. Jeong, K. Lee, J. Y. Park, Y. H. Ahn and S. Lee, *Carbon*, 2010, **48**, 2282.
25. W. S. Hummers and R. E. Offeman, *J. Am. Chem. Soc.*, 1958, **80**, 1339.
26. C. M. Shen, C. Hui, T. Z. Yang, C. W. Xiao, J. F. Tian, L. H. Bao, S. T. Chen, H. Ding and H. J. Gao, *Chem. Mat.*, 2008, **20**, 6939.
27. M. Chen, Y. G. Feng, X. Wang, T. C. Li, J. Y. Zhang and D. J. Qian, *Langmuir*, 2007, **23**, 5296.
28. K. S. Novoselov, A. K. Geim, S. V. Morozov, D. Jiang, Y. Zhang, S. V. Dubonos, I. V. Grigorieva and A. A. Firsov, *Science*, 2004, **306**, 666.
29. A. Thubagere and B. M. Reinhard, *ACS Nano*, 2010, **4**, 3611.
30. M. Auffan, J. Rose, J. Y. Bottero, G. V. Lowry, J. P. Jolivet and M. R. Wiesner, *Nat. Nanotechnol.*, 2009, **4**, 634.
31. S. Park, J. H. An, I. W. Jung, R. D. Piner, S. J. An, X. S. Li, A. Velamakanni and R. S. Ruoff, *Nano Lett.*, 2009, **9**, 1593.
32. X. Q. Fu, F. L. Bei, X. Wang, S. O'Brien and J. R. Lombardi, *Nanoscale*, 2010, **2**, 1461.
33. S. Park, N. Mohanty, J. W. Suk, A. Nagaraja, J. H. An, R. D. Piner, W. W. Cai, D. R. Dreyer, V. Berry and R. S. Ruoff, *Adv. Mater.*, 2010, **22**, 1736.
34. S. J. Ye, P. Majumdar, B. Chisholm, S. Stafslien and Z. Chen, *Langmuir*, 2010, **26**, 16455.